

## CRITICAL FLOW REGIONS IN THE CORONARY BY-PASS GRAFT ANASTOMOSIS

Alin F. TOTOREAN<sup>1</sup>, Alin I. BOSIOC<sup>1</sup>, Sandor I. BERNAD<sup>2</sup>, Romeo SUSAN-RESIGA<sup>1</sup>

<sup>1</sup> “Politehnica” University of Timisoara, Department of Mechanical Machines, Equipment and Transportation,  
RO-300222 Timisoara, Romania

<sup>2</sup> Romanian Academy, Centre of Fundamental and Advanced Research in Engineering Sciences, Timisoara Branch, 300223,  
E-mail: sandor.bernad@upt.ro

Aorto-coronary by-pass graft anastomosis geometry is complex, which causes strong secondary flow formation inside the region. Critical flow regions (recirculation regions and particle deposition) inside to the anastomosis zone are found in the current model. Experimental results show high secondary flow along the occluded artery and good fluid mixing distal to the anastomosis. Both investigated geometry: helical type and straight graft respectively shows same particle deposition in the critical region, around 8.5% of injected magnetic particle.

*Key words:* helical flow, by-pass graft, magnetic particle deposition, particle targeting.

### NOMENCLATURE

$B$	[T]	– Magnetic field	$U_m$	[m/s]	– mean axial velocity
$D$	[m]	– graft inlet diameter	$V_{in}$	[m/s]	– inlet velocity
$F_m$	[N]	– hidrodinamic force	$\alpha$	[°]	– angle of anastomosis
$m$	[Nm/T]	– magnetic momentum	$\rho$	[kg/m <sup>3</sup> ]	– fluid density
$p$	[Pa]	– pressure	$\nu$	[m <sup>2</sup> /s]	– kinematic viscosity
Re	[–]	– nondimensional Reynolds number	$\mu$	[Pa.s]	– dynamic viscosity

### 1. INTRODUCTION

After surgical intervention, coronary by-pass graft experimented two stresses: the blood flow induced stresses [1] and non-flow induced stresses (suture line wall stress) [2]. In the anastomotic region hemodynamic type of stresses regulate the function and dynamic remodeling, and also contribute to the development of pathological conditions [3, 4]. Blood flow in these regions is complex and is characterized by flow separation, stagnation, recirculation, turbulent flow, low shear stress in different areas [5, 6].

Artery bypass graft present conduit for severe artery stenosis diseases. Clinical statistics indicated that 10 years mortality rate of coronary artery bypass grafts (CABG) is 15%÷30% due to intimal hyperplasia (IH) resulting in post-operation restenosis and obstruction at distal anastomosis [7].

IH develops commonly in the distal anastomosis [8]. Both in vivo and vitro observations indicate that in the graft-artery anastomotic configuration, IH occurs preferentially around the suture-line [8, 9].

The phenomenon of spiral flow was observed in normal arteries [10]. Stonebridge *et al.* [11] further hypothesized that helical flow was helpful to endothelial damage repair.

In accordance with the viewpoints presented in [11] the spiral flow is a normal physiological flow phenomenon in arteries and can be helpful to endothelial damage repair. It is believed that helical flow can suppress the intimal hyperplasia development in coronary artery by-pass.

Encouraged by the findings of the preliminary research [12, 13] a novel CABG configuration is proposed and is hypothesized to have superior blood flow patterns for enhanced graft patency.

## 2. EXPERIMENTAL SETUP

### 2.1. GRAFT GEOMETRY

A steady-state flow in vitro model of an arterial bypass graft was used to examine the effects of the different geometry configuration on the flow patterns and the particle depositions in the distal anastomosis. Assembled experimental flow system provide the model with the desired inlet and outlet conditions.

A schematic of this system is shown in Fig. 1. The flow system consisted of a constant storage head tank; test section; floating ball flowmeter; collecting tank; and variable speed centrifugal pump. The mean flow rate was measured by a metric size ten rotameter with a stainless steel float. The rotameter leg served the extra purpose of preventing air from traveling upstream from the flow outlet. A blood analog fluid was prepared to have dynamic viscosity ( $\mu$ ) of 0.00408 Pa·s and a density ( $\rho$ ) of 1050 kg/m<sup>3</sup> (a glycerin-water mixture of 60% glycerine and 40% water).

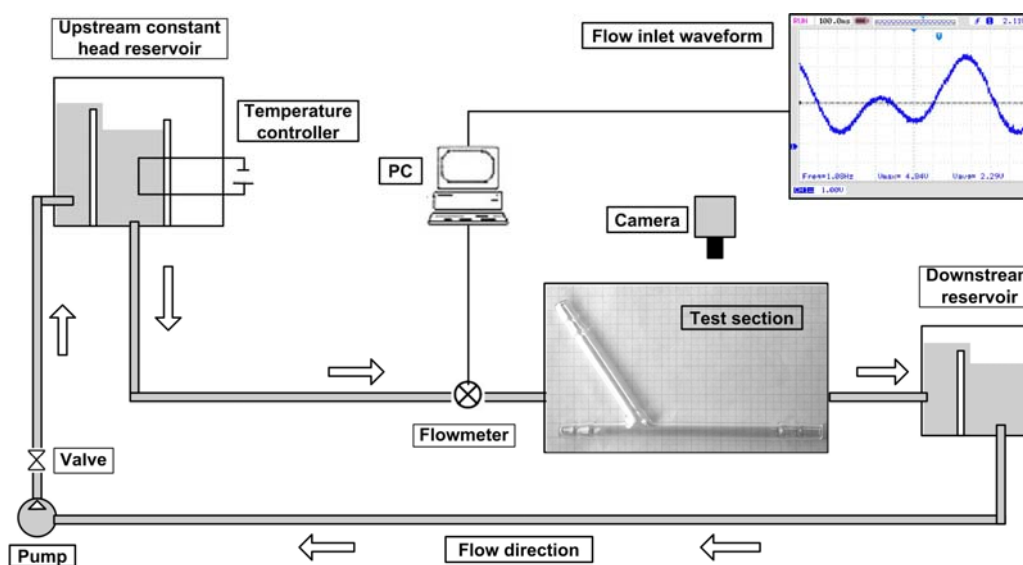


Fig. 1 – Experimental setup used for helical type graft investigations.

The geometric shape of the aorto-coronary bypass is shown in Fig. 2, and the geometric dimensions of the aorto-coronary bypass models are given in Table 1.

Flow experiment were conducted under typically physiological conditions [7]. The mean flow velocity is  $U_m = 0.144$  m/s. The mean Reynolds number, based on graft diameter and blood viscosity, is  $Re = 298$ .

Table 1

Bypass parameters (all parameters is given in mm)

Parameters	$Ls\_1/Lh\_1$ [mm]	$Ls\_2/Lh\_2$ [mm]	$Ls\_3/Lh\_3$ [mm]	$Ls\_4/Lh\_4$ [mm]
Straight by-pass	15	20	80	80
Two-turns helical by-pass	15	20	80	80

The experimental models were manufactured from glass tubing with constant internal diameter of 8mm, fashioned into a right shape and helical configuration with an approximately 80 mm straight segment proximally and 80 mm distally (Fig. 2). The both models are considered to have an anastomotic angle of 60° with the proximal segment of the coronary artery fully occluded. The models are designed to be planar.

For flow visualization study bolus of ink are injected into the water flowing at a different Reynolds numbers.

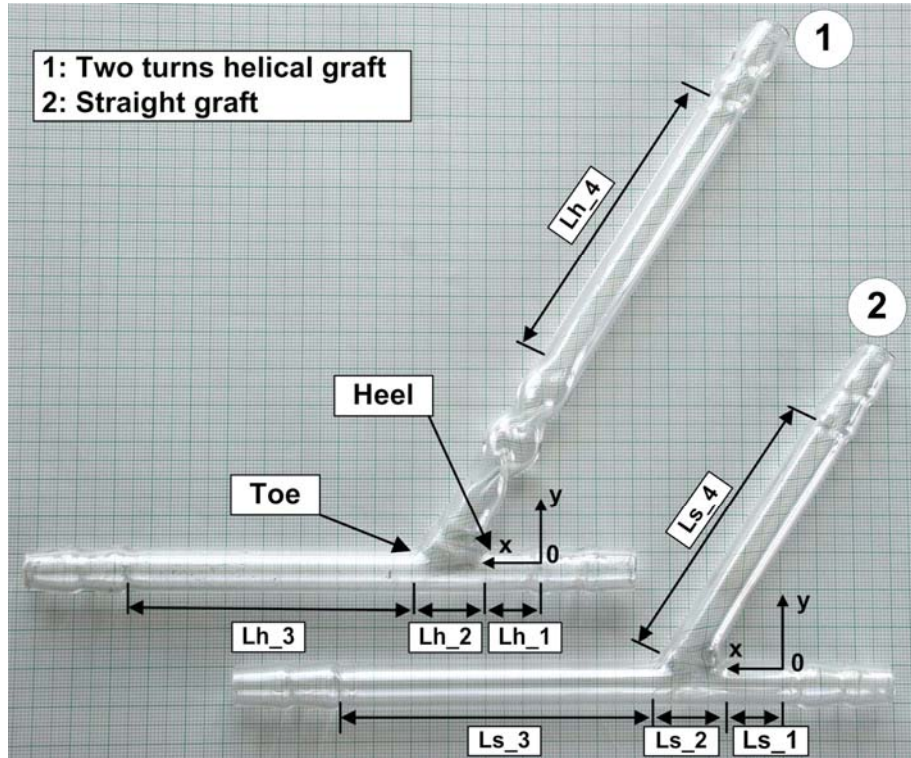


Fig. 2 – Experimental straight and helical bypass models manufactured from glass tubing with constant internal diameter of 8 mm (for both models) used for flow visualizations.

## 2.2. MAGNETIC TARGETING

One of the major challenge in the last period in terms of biomedical applications is to improve de chemotherapy efficiency using a more precise drugs concentration in the affected areas. Based on experiences accumulated in this area, idea were extended for other biomedical applications like treatment of the coronary artery pathology [14–17].

The general protocol for magnetic targeting involves exposure of the area of interest to an externally applied magnetic field, followed by the administration of magnetic particles (MNP's). After administration, nanoparticles were delivered to the area of interest by the fluid flow.

To compare the advantages of the suggested helical type bypass graft design over a conventional bypass graft configuration, magnetic particles deposition in anastomotic region are evaluated taking into account the effects of various parameters like: distance from the magnet, particle size, flow velocity.

The capture of magnetic particles was studied under steady-state flow condition ( $Re = 298$ ).

## 2.3. MAGNETIC PARTICLE

In order to evaluate de graft hydrodynamic performances of the ferromagnetic particles (FMP's) were used for quantification of particle deposition in anastomotic region. The ferromagnetic particles used during experimental investigations were iron particles with  $10\mu\text{m}$  in size (Merck KGaA, Darmstadt, Germany) and density of  $\rho = 7.87 \text{ g/cm}^3$ .

## 2.4. MAGNETIC FORCE ON A MAGNETIC PARTICLE

Hydrodynamic forces on a FMP arise due to differences in particle and fluid velocities. The magnetic force on a particle of magnetic moment  $m$ , acted upon by a magnetic field gradient  $\nabla B$ , can be expressed [18] as:

$$\vec{F}_m = \mu_0 \cdot (\vec{m} \cdot \nabla) \vec{H}_0 = \mu_0 \cdot m \cdot \nabla H_0, \quad (1)$$

where:

$$\vec{m} = \vec{m}(\vec{H}_0) = 4\pi\mu_0 \frac{\mu_p}{\mu_p + 2} \cdot a^3 \cdot \vec{H}_0, \quad (2)$$

where:  $\vec{H}_0$  – intensity of applied magnetic field and  $a$  – particle diameter.

In order to obtain the magnetic field gradient, we first took measurements of the magnetic field flux density within a region of interest ( $L \times W \times h = 116 \text{ mm} \times 56 \text{ mm} \times 5 \text{ mm}$  grid) perpendicular to the pole face of the test magnet (Fig. 3A). Figure 3B is a plot showing the magnetic field strength  $B$  within the measurement range. The vertical axis corresponds to the distance to the magnet's surface. It also indicates the axis of the magnet and the plot's axis of symmetry (Fig. 3A). The permanent magnet we used was a NdFeB magnet, the most widely used type of rare-earth magnet.

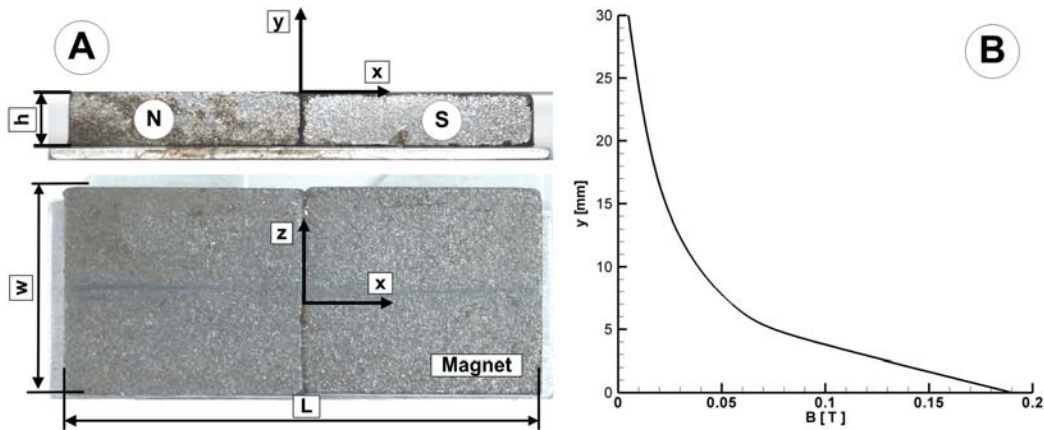


Fig. 3 – Magnet used for experimental measurements: A) magnet dimensions; B) magnetic field strength function of distance to the magnet surface. The origin correspond to the origin of axis indicated in A.

### 3. RESULTS AND DISCUSSION

#### 3.1. FLOW VISUALIZATION

In order to relieve the effect of the bypass geometry, all experiments were carried out under the same flow condition and graft angle. Steady flow ( $Re = 298$ ) in the 60-degree right and two-turn helical model is shown in Fig. 4.

Both geometries show the presence of the primary vortex in the proximal part of the host artery. The 60-degree model was particularly sensitive to particle deposition at the toe of the graft (vortex V1\_1 for straight graft and vortex V2\_1 for the two-turn helical graft shown in Figs. 4A and 4B).

Note the presence of the recirculation in the distal artery (Fig. 4A, vortex V1\_2 for straight graft) and stable flow in the helical bypass graft (Fig. 4B). The primary vortex that is the larger vortex (vortex V1\_1 and V2\_1, in both cases) closes to the anastomosis, rotated anti-clockwise as viewed in the photograph, whereas the more distal secondary vortex rotated clockwise (vortex V1\_2 in Fig. 4A).

The character of complex vortex structures created in the area between the heel and occluded part depends on the flow parameters. For straight by-pass graft, we can identify two vortices in the symmetry plane (vortex V1\_1 and V1\_2 – Fig. 4A). The shape of these vortices is strongly dependent on the occlusion distance from the anastomosis. The flow outside the symmetry plane moves in the form of a helical shaped vortex structure with variable spiral angle (Fig. 4A). These structures create secondary flow in the cross section [12]. The secondary flow intensity decreases downstream, and gradually, the velocity profile is formed into developed laminar velocity profile. There is an area with strong velocity gradient between the main flow and the vortex structure (Fig. 4A).

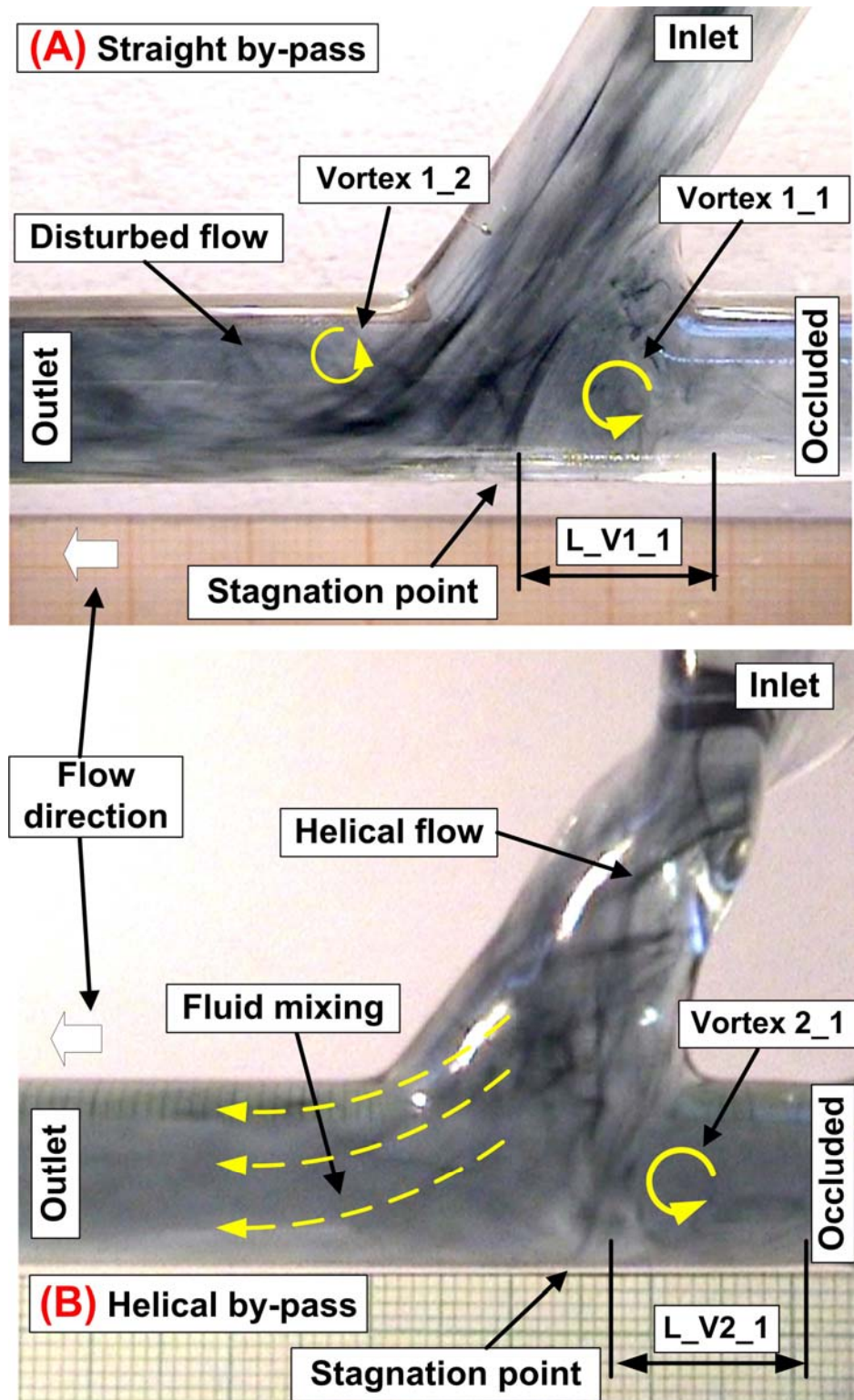


Fig. 4 – Experimental steady-state flow visualization (by-pass angle  $60^\circ$ ). For the same working condition helical type by-pass graft present a more conveniently flow structure namely: only one recirculation region, good fluid mixing and a short length of the main recirculation region.

In Fig. 4B, the absence of a recirculation region (due to the presence of the helical type graft) may be advantageous since this reduces the contact between blood and the artificial graft surface and, therefore, minimizes the risk of development of the IH and thrombosis.

### 3.2. MAGNETIC PARTICLE ACCUMULATION REGION

The key assumptions for the experimental investigations of the flow are: steady state flow, flow is laminar, gravitational effects are negligible, and physical properties remain constant.

Figure 5 shows the variation in magnet position and corresponding FMP accumulation in the by-pass anastomosis region. The axis of the magnet is always orthogonal to the branch-tube.

During experiments, it was detected that a high concentration of injected magnetic particles leads to accretions in the form of an elongated disc covering the outer wall of the anastomosis (Fig. 5).

Particles are only captured from flow when: 1) they are in contact with the artery wall, and 2) they have a zero velocity. Moreover, since particles at rest in a moving fluid experience a drag force, there must be a component of the magnetic force of sufficient strength to overcome the drag in order to retain a particle.

Accumulation of FMP during magnetic targeting results in a reduction of the cross-sectional area of the artery (i.e. FMP accumulation plugs a section of the anastomosis) resulting a change in fluid velocity.

Photographic images of FMP retention in the anastomosis region for different magnet position are shown in Fig. 5. For both by-pass geometries, particles were seen to accumulate in low lying “dunes” running across the entire pole face of the magnet and slightly increased accumulation downstream from the center.

Figure 5 shows the FMP’s concentration after the final steady-state flow condition has been reached corresponding to the different magnetic field intensities of B (Table 2). In this scenario, the magnet axis has a distance of 8 mm from the by-pass branch-point and at the maximum of 15 mm from the host artery axis. The profiles clearly show the influence of the magnetic field. In the left profile (noted S1, S2 and S3 respectively) can see that the FMP is attracted to the outer wall of the anastomosis and have a symmetric distribution along the magnet axis. For helical type by-pass graft (profile b, noted with H1, H2 and H3) a considerable higher FMP concentration are present in the distal part of the anastomosis.

Since magnetic field gradients drop sharply with distance from the magnet, MNP retention would also depend on the magnetic field intensity.

Quantitative analysis (Fig. 5 and Table 2), showed that  $15.9 \pm 2.6\%$  and  $85.4 \pm 0.6\%$  of FMP are retained in the straight and the helical type by-pass respectively.

Table 2

Magnetic particle deposition (Fig. 5)

Nr.	Position	Magnet distance from axis of the host artery mm]	FMP percentage accumulation in straight graft [%]	FMP percentage accumulation in helical graft [g]	Flow condition	By-pass angle
1	P1	7	8.692	9.888	steady-state	60°
2	P2	10	8.106	8.486	steady-state	60°

## 4. CONCLUSIONS

The critical flow regions, which may cause the formation of intimal hyperplasia and finally blockage inside this connection was identified in the anastomosis region of the by-pass.

The experimental results demonstrate that the new by-pass model provides:

- (i) an uniform flow in the anastomosis region, without vortex formation in the heel region;
- (ii) less flow recirculation and stagnation on the artery bed of the helical model as compared to the straight model;
- (iii) FMP’s deposition clearly shows that the helical by-pas model can reduce the probability of IH and atherosclerotic lesion development at these critical anastomotic sites (more favorable flow structure and fluid mixing in case of helical graft over against particle depositions tendency presented in Table 2).

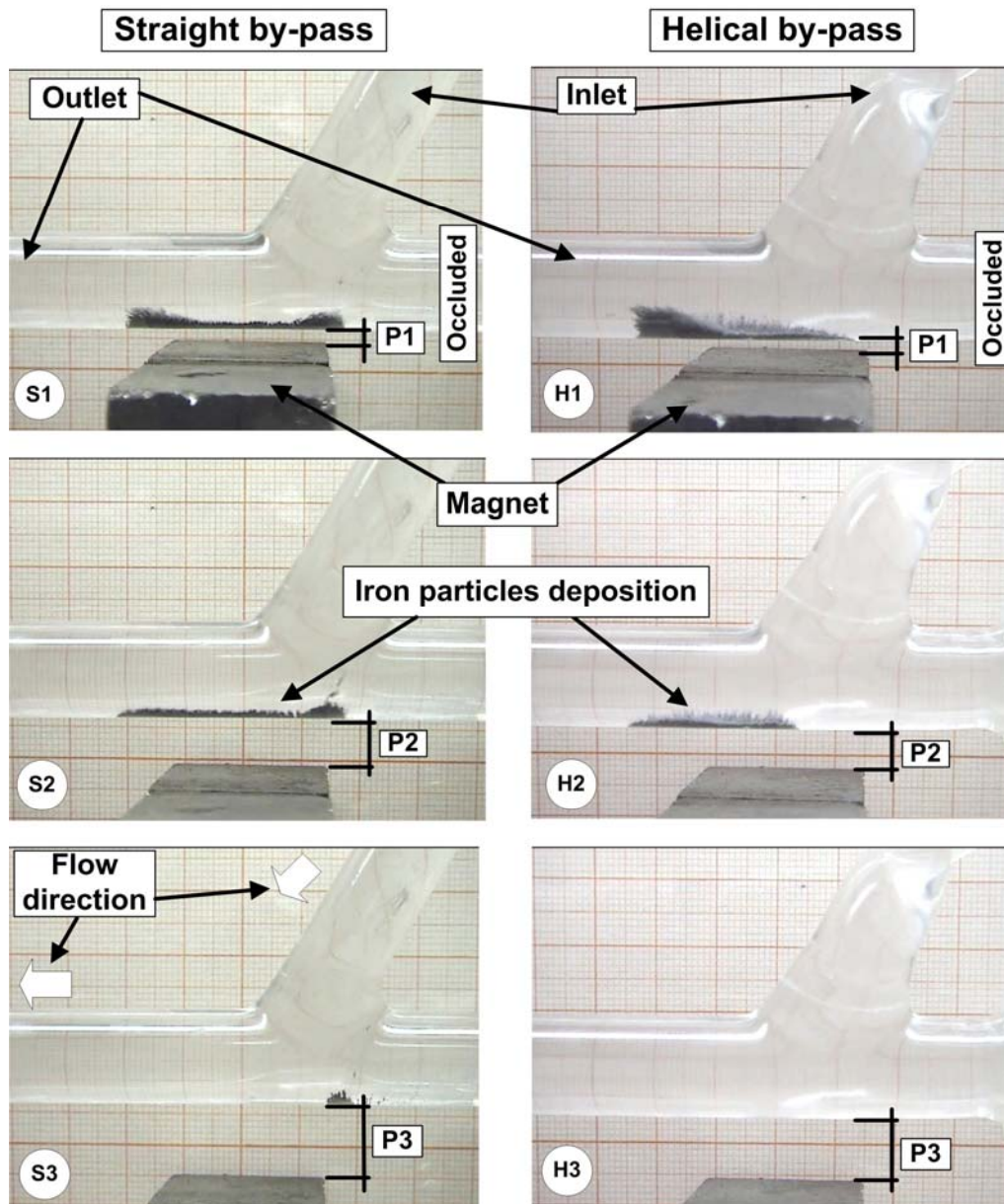


Fig. 5 – Magnetic particles accumulations in the anastomotic region of the by-pass graft, for different magnetic field intensity (different magnet position).

### ACKNOWLEDGMENTS

This work has been supported by Romanian Academy annual program and for A. F. Totorean, this work was partially supported by the strategic grant POSDRU/159/1.5/S/137070 (2014) of the Ministry of National Education, Romania, co-financed by the European Social Fund – Investing in People, within the Sectoral Operational Programme Human Resources Development 2007-2013.

### REFERENCES

1. HARUGUCHI H., TERAOKA S., *Intimal hyperplasia and hemodynamic factors in arterial bypass and arteriovenous grafts: a review*, J. Artif. Organs, **6**, pp. 227–235, 2003.
2. BALLYK P.D., WALSH C., BUTANY J., OHJA M., *Compliance mismatch may promote graft-artery intimal hyperplasia by altering suture-line stresses*, J. Biomech., **31**, pp. 229–237, 1998.

3. KAKISIS J.D., LIAPIS C.D., SUMPIO B.E., *Effects of cyclic strain on vascular cells*, *Endothelium*, **11**, 1, pp. 17–28, 2004.
4. SHIU Y.T., *Mechanical forces on cells*. In: Bronzino JD (ed). *The Biomedical Engineering Handbook: Tissue Engineering and Artificial Organs*, 3rd ed., CRC Press Taylor & Francis Group, LLC: Boca Raton, 2006, pp. 33.31–33.18.
5. KRUEGER U., ZANOW J., SCHOLZ H., *Computational fluid dynamics and vascular access*, *Artif. Organs*, **26**, pp. 571–575, 2002.
6. MIGLIAVACCA F., DUBINI G., *Computational modeling of vascular anastomoses*, *Biomech. Model Mechanobiol.*, **3**, pp. 235–250, 2005.
7. SHAPIRA I., ISAKOV A., HELLER I., TOPILSKY M., PINES A., *Longterm follow up after coronary artery bypass grafting reoperation*, *Chest*, **115**, 6, pp. 1593–1597, 1999.
8. BALLYK P.D., WALSH C., BUTANY J., OJHA M., *Compliance mismatch may promote graft\_artery intimal hyperplasia by altering suture-line stresses*, *J. Biomech.*, **31**, 3, pp. 229–237, 1998.
9. BASSIOUNY H.S., WHITE S., GLAGOV S., CHOI E., GIDDENS D.P., ZARINS C.K., *Anastomotic intimal hyperplasia: mechanical injury or flow induced*, *J. Vasc. Surg.* **15**, 4, pp. 708–717, 1992.
10. UCHIDA Y., TOMARU T., NAKAMURA F., FURUSE A., FUJIMORI Y., HASEGAWA K., *Percutaneous coronary angiography in patients with ischemic heart disease*, *AmHeart J.*, **114**, pp. 1216–1222, 1987.
11. STONEBRIDGE P.A., BROPHY C.M., *Spiral laminar flow in arteries?* *Lancet*, **338**, pp.1360, 1991.
12. TOTOREAN A.F., BOSIOC A.I., BERNAD S.I., SUSAN-RESIGA R., *Identification and visualization of vortices in by-pass graft flow*, *Proceedings of the Romanian Academy Series A*, **15**, 1, pp. 52–59, 2014.
13. BERNAD S.I., BOSIOC A., BERNAD E.S., CRAINA M.L., *Comparison between experimentally measured flow patterns for straight and helical graft*, *Bio-Medical Materials and Engineering*, **24**, pp. 853–860, 2014.
14. BALI R., AWASTHI U., *Effect of a magnetic field on the resistance to blood flow through stenotic artery*, *Applied Mathematics and Computation*, **188**, pp. 1635–1641, 2007.
15. KHASHAN S.A., HAIK Y., *Numerical simulation of biomagnetic fluid downstream an eccentric stenotic orifice.*, *Physics of Fluids*, **18**, 11, pp. 113601, 2006.
16. CHERRY E.M., MAXIM P.G., EATON J.K., *Particle size, magnetic field, and blood velocity effects on particle retention in magnetic drug targeting*, *Med. Phys.*, **37**, 1, pp. 175–182, 2010.
17. ALLAN E., ADAM D.,J. CHERTOK C.B., PARK Y.S., YANG V.C., *A combined theoretical and in vitro modeling approach for predicting the magnetic capture and retention of magnetic nanoparticles in vivo*, *Journal of Controlled Release*, **152**, pp. 67–75, 2011.
18. BOSSIS G., VOLKOVA O., LACIS S., MEUNIER A., *Magnetoreology: Fluids, Structures and Rheology*, in S. odenbach (Ed), *Ferofluids. Magnetically controllable fluids and their applications*, *Lecture Notes in Physics*, **594**, pp. 202–230, 2002.

Received, November 10, 2014